Lasers in Medical Science (2019) 34:1849–1855
https://doi.org/10.1007/s10103-019-02781-w

ORIGINAL ARTICLE

Label-free diagnosis of lung cancer with tissue-slice surface-enhanced Raman spectroscopy and statistical analysis

Kun Zhang[1] · Chunyan Hao[2] · Yanyan Huo[1] · Baoyuan Man[1] · Chao Zhang[1] · Cheng Yang[1] · Mei Liu[1] · Chuansong Chen[1]

Received: 6 December 2018 / Accepted: 27 March 2019 / Published online: 13 April 2019

Abstract
Despite the rapid development of medical science, the diagnosis of lung cancer is still quite challenging. Due to the ultrahigh detection sensitivity of surface-enhanced Raman spectroscopy (SERS), SERS has a broad application prospect in biomedicine, especially in the field of tumor blood detection. Although Raman spectroscopy can diagnose lung cancer through tissue slices, its weak cross sections are problematic. In this study, silver nanoparticles (AgNPs) were added to the surface of lung tissue slices to enhance the Raman scattering signals of biomolecules. The electromagnetic field distribution of AgNPs prepared was simulated using the COMSOL software. SERS obtained from the slices reflected the difference in biochemical molecules between normal ($n = 23$) and cancerous ($n = 23$) lung tissues. Principal component-linear discriminate analysis (PCA-LDA) was utilized to classify lung cancer and healthy lung tissues. The receiver operating characteristic curve gave the sensitivity (95.7%) and specificity (95.7%) of the PCA-LDA method. This study sheds new light on the general applicability of SERS analysis of tissue slices in clinical trials.

Keywords Surface-enhanced Raman spectroscopy (SERS) · Silver nanoparticles · Tissue slice · Lung cancer · PCA-LDA

Introduction

Timely diagnosis and effective treatment of lung cancer are the linchpin of improved survival rates for cancer patients. However, the actual detection methods including computed tomography (CT) and positron emission tomography (PET) have considerable limitations, which affect their diagnostic effectiveness for lung cancer [1, 2]. Therefore, there is an urgent need for a fast, accurate, relatively inexpensive, and noninvasive method for detection of lung cancer. Raman spectroscopy can characterize biomolecules, because each macromolecule (lipid, protein, DNA, etc.) has unique fingerprinting information about the modes of vibration and rotation [3]. Therefore, Raman spectroscopy will become a promising tool for cancer diagnostics in the future. Nevertheless, Raman spectroscopy has the deficiency of low sensitivity in practical application. Compared with conventional Raman spectroscopy, Raman scattering signals can be strengthened by 4–15 orders of magnitude utilizing surface-enhanced Raman spectroscopy (SERS) technology [4–6]. In recent years, SERS has shown great application potential in biomarker detection, as well as for in vivo tumor localization and detection [7, 8].

So far, SERS technology has made remarkable achievements in the field of biomolecule detection [5, 6]. The intensity of SERS is linked to the material and morphology of the metal particles. Studies have shown that the Raman enhancement effect can be obtained by utilizing silver nanospheres [9], gold nanospheres [10], and so forth. Moreover, SERS based on silver nanoparticles (AgNPs) as a substrate has achieved rapid detection and identification of pathogenic bacteria [11]. Park et al. distinguished lung cancer and normal cell-derived exosomes by SERS and statistical methods [12]. Li et al. utilized silver colloids as a substrate to acquire

Electronic supplementary material The online version of this article (https://doi.org/10.1007/s10103-019-02781-w) contains supplementary material, which is available to authorized users.

✉ Chuansong Chen
chencs@sdnu.edu.cn

[1] Shandong Province Key Laboratory of Medical Physics and Image Processing Technology, School of Physics and Electronics, Shandong Normal University, Jinan 250014, China

[2] Key Laboratory of the Ministry of Education for Experimental Teratology, Department of Histology and Embryology, School of Medicine, Shandong University, Jinan 250012, China

salivary SERS [13]. They found that protein and nucleic acid levels were significantly reduced in cancer patients, and the feasibility of salivary SERS measurements for the diagnosis of lung cancer was demonstrated using principal component analysis (PCA) and linear discriminate analysis (LDA). However, other studies have shown that the contents of nucleic acid and protein in lung cancer cells were increased, based on Raman spectroscopy [14, 15]. Therefore, SERS technology has broad prospects in the diagnosis of lung cancer, and it is necessary to carry out in-depth exploration of lung cancer at the molecular level.

Tissue samples are one of necessary materials for cancer diagnosis. In clinical detection, label-free SERS detection of tissue provides a rapid and facile way to differentiate tumors from normal tissues [16]. In this paper, we used AgNPs as SERS substrate to discriminate the tissue sections of lung cancer patients from the controls, providing new clues for the universal applicability of SERS in the clinical diagnosis of lung cancer. To avoid the effect of differences in patients overwhelming the differences between cancerous and healthy tissue in experimental measurement results, we conducted the collection of SERS data from a large number of patients. PCA combined with LDA was utilized to diagnose and classify the tissue-section SERS acquired from cancerous and normal tissues. The receiver operating characteristic (ROC) curves further verifies the veracity of the PCA-LDA-based diagnostic algorithm. Furthermore, the changes of biological components caused by tissue carcinogenesis can be clearly demonstrated through SERS analysis of the tissue slices. The new method demonstrated that tissue sections SERS based on AgNPs-substrates has an extensive prospect in the detection and analysis of lung cancer.

Materials and methods

Preparation of sliver nanoparticles

In this study, the stable Ag colloid solutions were prepared following the protocol reported by Zhang et al. [17]. AgNPs were synthesized in a liquid phase by combining silver nitrate ($AgNO_3$, 0.1 g), polyvinylpyrrolidone (PVP, 2.5 g, Mw = 55,000), and ethylene glycol ($C_2H_6O_2$, 20 mL, 99%). All the reagents were of analytical grade, purchased from Sinopharm Chemical Reagent Co., Ltd. in China.

Sample preparation

Tissue sections were prepared according to standard-embedded protocols [18]. To avoid the effect of paraffin on the test results, for de-paraffinization, a standard histological protocol was used. Experimental samples originating from cancerous and normal lung tissues of each patient were obtained, and the detailed information about the clinical and histopathological diagnoses of each patient is listed in Table S1. Twenty-three patients ranged in the age from 38 to 72 years old, including 8 females and 15 males. For all patients with lung cancer, there were 11 patients with clinical stage III and 12 patients with clinical stage IV. Samples for SERS detection were divided into two groups: one group has 23 lung cancerous slices from 23 patients, while the other has 23 normal ones from 23 patients. The sample collection was subject to approval by the doctor and patient, and also approved by the medical ethics committee of Qilu Hospital of Shandong University. All tissue slices were first diagnosed by pathologists. Next, AgNPs were added to the surfaces of tissue slices, and the SERS signal was acquired subsequently.

SERS measurements

The Raman detection system (Horiba, France, Horiba HR Evolution 800) with an excitation wavelength of 532 nm was used to acquire SERS data. The laser beam was focused on the sample surface by a × 50 objective (N.A. = 0.5) through external and internal light path transmission systems. The size of laser excitation spot on the surface of samples was 1 μm. SERS data were conducted on each sample (60 μm × 60 μm regions, 6 × 6 points) by Raman detection system (800–1800 cm^{-1} spectral range, 4 s integration times, 0.5-mW laser power and 600 lines mm^{-1} diffraction grating), and quantitatively analyzed using Origin (OriginLab, America, Origin software 8.5). To prevent the influence of natural light on the experimental results, the spectral acquisition was carried out in a dark environment.

Data processing

As the entire SERS data sets have more variables, LDA and PCA are coupled to minimize the complexity and dimensionality of spectral data. Firstly, the fluorescence background of the original SERS data was removed using a multi-polynomial fitting algorithm. Then, each spectrum was normalized by the integrated area under the curve. After that, data in the spectral range was fed into the SPSS software package (IBM, America, SPSS Statistics 19.0) for PCA-LDA analysis [19].

Results and discussion

Sliver nanoparticle measurements

Sample images obtained by scanning electron microscopy (SEM, Zeiss, Germany, Zeiss Gemini Ultra-55) are shown in Fig. 1a–d. Well-distributed AgNPs are clearly observed (Fig. 1a–c), which have a relatively regular size with only minor deviations. The gap between the silver nanoparticles is about

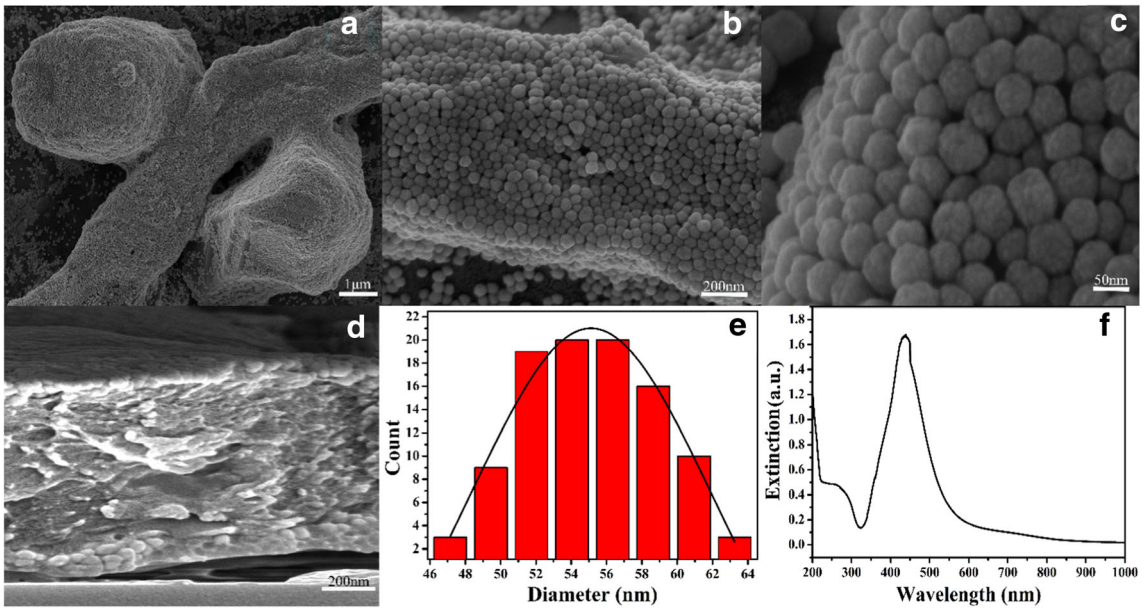

Fig. 1 SEM images with various magnifications of a lung tissue slice covered with AgNPs. Magnifications. **a** × 10,000, **b** × 50,000, and **c** × 200,000. **d** The cross-sectional side view image of the sample covered with AgNPs. **e** Diameter statistics images of AgNPs; the diameter is about 55 nm. **f** The UV-Vis extinction spectrum of the pure Ag colloid

4 nm. The cross section in Fig. 1d was measured to investigate the surface morphology of AgNPs on the surface of the tissue slices. This provides direct evidence that the distribution of AgNPs on the surface is mostly in one layer or two layers. We utilized the Nano Measurer software to measure the size of the nanometer particle, and the mean diameter of the particles is about 55 nm (Fig. 1e). The peak of the AgNPs extinction as measured by UV-Vis spectrometer (Hitachi, Japan, Hitachi U-4000) is at 437 nm, as shown in Fig. 1f. Figure 3(a) shows some strong SERS signals while that in Fig. 3(b) are weak, which suggests that Raman bands are enhanced significantly by adding AgNPs to the surface of the sample. As we all know, hot spots are significant to electromagnetic mechanism. Therefore, the dense hot spots of the nano-gap is a direct evidence to prove the electromagnetic field enhancement. At the same time, the simulation results of COMSOL can be used as an auxiliary proof for the enhancement of biomolecule Raman scattering signals. In order to further investigate the strong Raman enhancement effect of AgNPs prepared by the sol-gel method, the electromagnetic field distribution of AgNPs (55 nm in diameter, with 4-nm spacing gaps) on the SiO_2 substrate was simulated using the COMSOL software (COMSOL, Sweden, COMSOL Multiphysics software) (Fig. 2). Figures 2a and b are the theoretical simulated images in the *Y-Z* plane for one-layer and two-layer AgNPs, respectively. The coupling effect of surface plasmons makes the gaps of the AgNPs appear as hot spots with high electric field intensity, and the local electric field is also obviously enhanced in the contact area of the AgNPs and sample. The above results show that the prepared sample has a strong Raman enhancement effect, facilitating the collection of more biochemical spectral information.

To demonstrate the enhanced effect of AgNPs on Raman scattering of tissue samples, we measured the SERS data and Raman spectra of normal and lung cancerous tissues. Raman spectra and SERS were collected from the lung tissue section of the same patient under the same instrumentation set-up to ensure the accuracy of the experiment (Fig. 3). Figure 3(a–c)

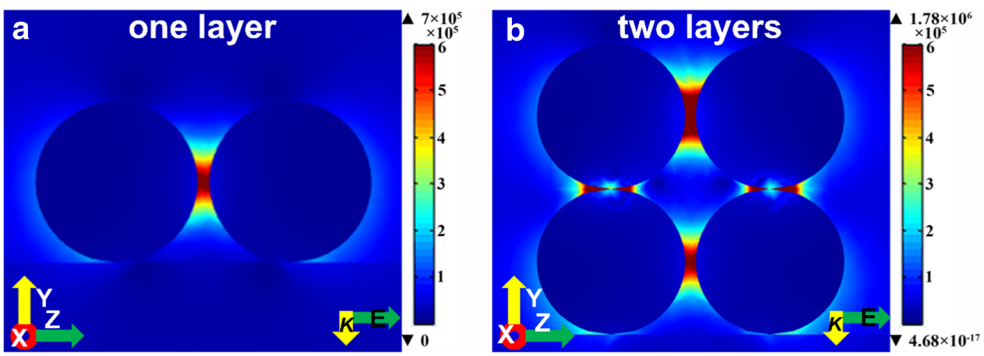

Fig. 2 **a**, **b** COMSOL simulation of local electric field distribution for AgNPs in the *Y-Z* plane with 532 nm incident light

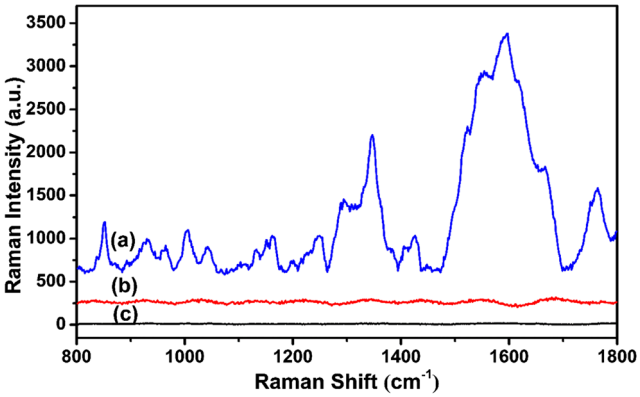

Fig. 3 (a) SERS of the tissue slice sample, covered with AgNPs, from a patient with lung cancer. (b) Raman spectrum of the same tissue slice sample without AgNPs. (c) the Raman signal of AgNPs

shows the SERS of the lung tissue surface with AgNPs, the Raman spectrum without AgNPs, and the Raman spectrum of the isolated AgNPs. Figure 3(a) shows some strong SERS signals while that in Fig. 3(b) are weak, which suggests that Raman bands are enhanced significantly by adding AgNPs to the surface of the sample. In Fig. 3(c), there is no Raman peak in the detection area, indicating that the AgNPs applied in this experiment are relatively pure and do not affect the SERS signal of the sample. In the theoretical simulation part, we have proved the reason for the enhancement of the Raman scattering signal, and experimental results agree well with the theoretical simulation ones.

SERS measurements

To better show the difference in material composition between cancerous and normal lung tissues, large amounts of SERS data were acquired. The normalization of spectral data can reduce the interference caused by spectral intensity in the succeeding analysis. Figure 4a shows mean SERS data and standard deviations obtained from 23 normal lung tissues and 23 cancerous ones. The solid line represents mean SERS, and the shaded region represents the standard deviation. Differences in SERS data between cancerous tissues and normal ones are shown in Fig. 4b, and we can see the difference between the cancerous and normal tissues at around 830, 913, 1001, 1057, 1074, 1089, 1152, 1184, 1216, 1239, 1287, 1317, 1360, 1378, 1395, 1421, 1453, 1514, 1564, 1585, 1601, 1628, 1652, and 1700 cm^{-1}. In Table S2, we intuitively describe the spectral bands obtained from measurement. The differences in SERS spectra between lung cancer and normal tissues show that there is considerable potential for diagnosis of lung cancer with tissue SERS.

Compared with normal lung tissues, the contents and conformations of components in cancerous tissue such as DNA, proteins, and lipids may generate subtle changes. To better analyze SERS characteristics of biomolecules in lung tissue,

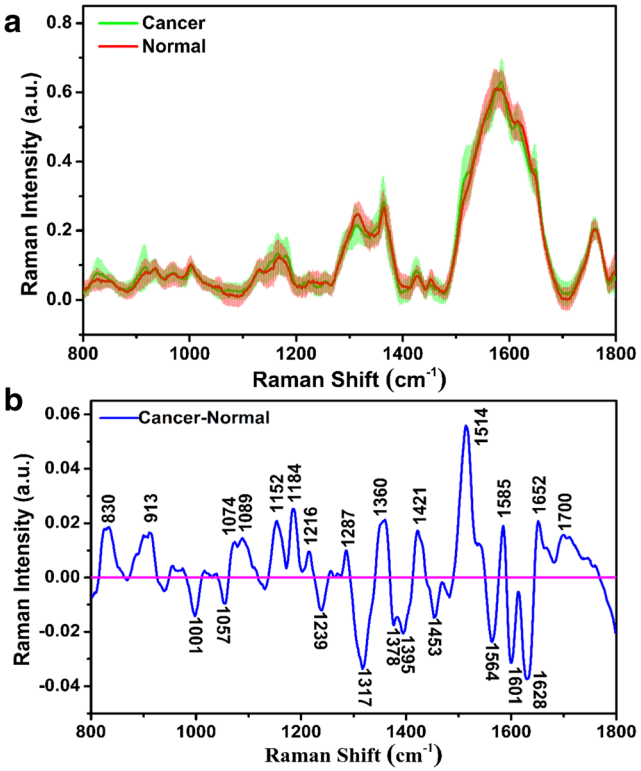

Fig. 4 **a** Mean SERS for the lung cancer ($n = 23$) and normal ($n = 23$) tissue slices. The shaded areas represent the standard deviations of the means. **b** The difference spectrum of the cancer-normal SERS

we tentatively assign the SERS data obtained from the experiment, as listed in Table 1 [14, 20–25]. SERS of the cancerous tissue are heavily enhanced at around 830 (C-H out of plane bending), 1074 (symmetric PO_2^- stretching), 1089 (C-C stretching), 1152 (C = C stretching), 1216 (C-N stretching), 1287 (CH contortion), 1360 (C = O stretching), 1421 (ring breathing), 1514 (C = C stretching), 1585 (C = C stretching), 1652 (C = C stretching), and 1700 cm^{-1} (C = O stretching), while SERS of the normal tissues are significantly strengthened at around 1001 (C-C skeletal), 1239 (N-H surface deformation), 1317 (ring vibration), 1378 (C-H ring asymmetric), 1395 (symmetric COO^-), 1453 (C-H bending), 1564 (COO^-), 1601 (C = O stretching), and 1628 cm^{-1} (C = O stretching). The SERS peaks at 830, 1152, 1317, 1421, and 1601 cm^{-1} were also reported in Raman studies of lung cancer [14, 15, 26]. Therefore, our interpretations of the experimental data by the difference spectrum are justified. One of the most striking aspects of comparison are the marked differences in the SERS spectra for glucose (913 cm^{-1}), DNA (1079 and 1421 cm^{-1}), carotenoids (1152 and 1514 cm^{-1}), lipids (1089, 1453, and 1652 cm^{-1}), and proteins (1152, 1453, and 1585 cm^{-1}). Relative SERS peak intensity at 913 cm^{-1} for glucose is deemed to be higher in lung cancerous tissue than in normal tissue. Moreover, this peak was found to be a marker of the abnormal glucose metabolism in cancer tissue [27]. Compared to healthy subjects, DNA has been reported in considerably

Table 1 SERS peak positions and vibrational mode assignments

Peak position (cm^{-1})	Vibrational mode	Major assignment
830	C-H out of plane bending	Proline, hydroxyproline, tyrosine
913	Not stipulated attribution	Glucose
1001	C-C skeletal	Phenylalanine
1057	Not stipulated attribution	Lipids
1074	Symmetric PO_2^- stretching	DNA
1089	C-C stretching	Lipids
1152	C = C stretching	Proteins, carotenoid
1184	Not stipulated attribution	Cytosine, guanine, adenine
1216	C-N stretching	Not stipulated attribution
1239	N-H surface deformation	Amide III
1287	CH contorting	Cytosine
1317	Ring vibrational	Guanine
1360	C =O stretching	Tryptophan
1378	C-H ring asymmetric	Paraffin
1395	Symmetric COO^-	Carboxylate
1421	Ring breathing	Deoxyribose, DNA/RNA
1453	C-H bending	Protein, structural protein
1514	C = C stretching	Carotenoid
1564	COO^-	Not stipulated attribution
1585	C = C olefinic stretching	Protein
1601	C = O stretching	Amide I
1628	C = O stretching	Amide I
1652	C = C stretching	Lipids
1700	C = O stretching	Amino acids aspartic, glutamic acid

higher concentrations in other malignancies (esophageal, breast, liver, etc.) [28]. The strong SERS peak appearing at 1089 (C-C stretching), 1453 (C-H bending), and 1652 cm^{-1} (C = C stretching) further confirmed the change of the biological molecular content with tumor transformations. Enhanced lipid contents are observed in cancerous tissues compared with the normal tissues. The cancerous lung tissue contains much more adipose and proteins, which may be associated with hydrophilicity and hydrophobicity of the tissues. The larger content of protein and DNA in cancerous tissues had also been confirmed by gastric and colon cancer studies [29, 30]. Figure 4 and Table 1 demonstrate that the cancerous lung tissue contains a markedly higher concentration of carotenoids (1152 and 1514 cm^{-1}) due to the higher C = C stretching vibration intensities than those of the control tissue. In contrast with studies of lymphocytes, the intensity of band at 1152 and 1514 cm^{-1} in the tissue SERS of lung was increased; this may be due to the differences in carotenoid metabolism between different tissues. Guanine (1317 cm^{-1}) is the basic unit of nucleic acid; the decrease of its concentration indicates a

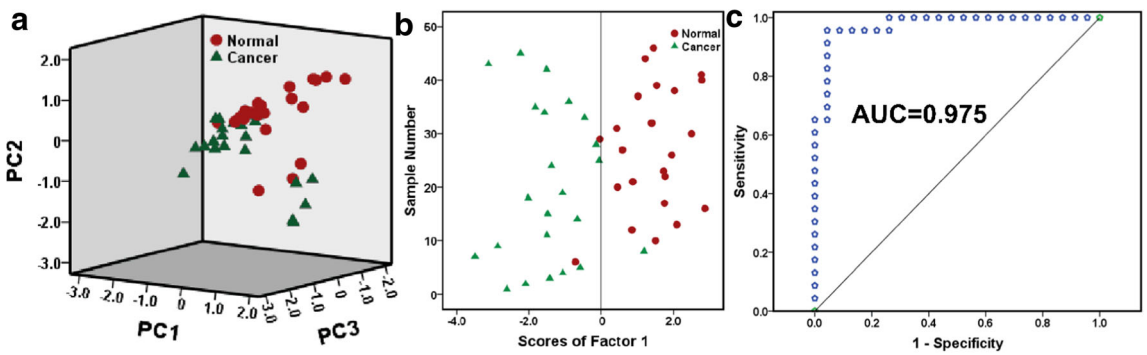

Fig. 5 **a** Scatter plot of PC1, PC2, and PC3 for normal ($n = 23$) and cancerous ($n = 23$) tissue slices. **b** Scatter plots of the posterior probability for the normal and lung cancer categories calculated from the data sets, using PCA-LDA-based spectral classification. **c** The ROC curve of the discrimination diagnostic result for using PCA–LDA-based SERS classification

decrease of nucleic acid content. This trend of decreasing may be induced by the breakdown of several kinds of molecular bonds. The decrease in nucleic acid content of lung cancer patients has also been confirmed in Li et al. [13]. In summary, it can be observed that SERS can distinguish between cancerous tissues and normal lung tissues.

Multivariate statistical analysis

PCA-LDA has been used in the classification of SERS in disease diagnosis and has obtained highly accurate prediction results [8, 13]. To test the detailed spectral differences of lung SERS for cancer and normal tissues, PCA-LDA was performed on the measured SERS of the tissue sections. Briefly, the PCA-LDA was performed based on the entire processed SERS spectra set using the SPSS program. The first three principal components (PCs; PC1 35.6%, PC2 23.3%, and PC3 10.8% ($p < 0.05$)) have the greatest variance, together accounting for 70% of all the variance. Figure 5 a shows a scatter plot of PC1, PC2, and PC3 for normal and cancerous tissues. We found that the data points for the cancerous and normal samples form distinct, separated clusters, which mean that SERS allow discrimination between the lung cancerous and normal lung tissues. To incorporate all significant SERS spectral features, LDA is utilized to generate diagnostic algorithms using the PC scores for the first 12 PCs (PC1–PC12, 95%). Figure 5b shows the posterior probabilities of the normal and lung cancer tissues as calculated by the LDA method. To examine the applicability, the ROC curve is constructed (Fig. 5c). The integrated area under the curve (AUC) of a ROC curve is 0.975 for PCA-LDA-based diagnostic algorithms, which indicates efficient performance of these diagnostic models. Therefore, the cancer tissue slices could be unambiguously discriminated from the normal ones, leading to 95.7% diagnostic sensitivity as well as specificity, and thus demonstrating the potential of SERS as a clinical tool for label-free lung cancer detection.

Conclusion

In summary, AgNPs-based SERS was implemented to analyze tissue sections from cancerous and normal lung tissues. After the initial allocation of SERS, we found that there are considerable differences in the biological molecular content between cancerous and normal tissues. Tentative assignment of the SERS data reflects lung tissue biomolecular changes with cancer, including an increase in the relative amounts of DNA, carotenoids, lipids, and proteins, and a decrease in the percentage of nucleic acid content in the tissue sections of lung cancer tissues compared to that of normal lung tissues. PCA-LDA can divide the tissue samples into distinct clusters for the two groups: cancerous versus normal lung tissue slices. The sensitivity and specificity were 95.7% and 95.7%, respectively. These results showed that the tissue-slice SERS analysis may be of great importance for the label-free detection and screening of lung cancer. Our next step will be to use functionalized nanoparticles to perform more accurate targeted real-time detection of tumor tissue cells in vivo.

Funding information This work was supported by the National Natural Science Foundation of China (11774208, 11674199, and 11604040), Shandong Province Natural Science Foundation (ZR2018MA040, ZR2017BA004, ZR2016AM19), China Postdoctoral Science Foundation (2016M602716).

Compliance with ethical standards

Conflict of interest The authors declare that they have no conflicts of interest.

Ethics statement The sample collection was approved by the medical ethics committee of Qilu Hospital of Shandong University.

Informed consent Informed consent was obtained from all individual participants included in the study.

References

1. Bird RE, Wallace TW, Yankaskas BC (1992) Analysis of cancers missed at screening mammography. Radiology 184(3):613–617
2. Berrington de Gonzalez A, Berg CD, Visvanathan K et al (2009) Estimated risk of radiation-induced breast cancer from mammographic screening for young BRCA mutation carriers. J Natl Cancer I 101(3):205–209
3. Kudelski A (2008) Analytical applications of Raman spectroscopy. Talanta 76(1):1–8
4. Shao J, Tong L, Tang S et al (2015) PLLA nanofibrous paper-based plasmonic substrate with tailored hydrophilicity for focusing SERS detection. ACS Appl Mater Inter 7(9):5391–5399
5. Li Z, Wang M, Jiao Y et al (2018) Different number of silver nanoparticles layers for surface enhanced raman spectroscopy analysis. Sensor Actuat B Chem 255:374–383
6. Zhang C, Jiang S, Huo Y et al (2015) SERS detection of R6G based on a novel graphene oxide/silver nanoparticles/silicon pyramid arrays structure. Opt Express 23(19):24811–24821
7. Huang X, El-Sayed IH, Qian W et al (2007) Cancer cells assemble and align gold nanorods conjugated to antibodies to produce highly enhanced, sharp, and polarized surface Raman spectra: a potential cancer diagnostic marker. Nano Lett 7(6):1591–1597
8. Petersen D, Mavarani L, Niedieker D et al (2017) Virtual staining of colon cancer tissue by label-free Raman micro-spectroscopy. Analyst 142(8):1207–1215
9. Zhou H, Yang D, Ivleva NP et al (2015) Label-free in situ discrimination of live and dead bacteria by surface-enhanced Raman scattering. Anal Chem 87(13):6553–6561
10. Wang X, Qian X, Beitler JJ et al (2011) Detection of circulating tumor cells in human peripheral blood using surface-enhanced Raman scattering nanoparticles. Cancer Res 71(5):1526–1532
11. Dina N, Zhou H, Colniță A et al (2017) Rapid single-cell detection and identification of pathogens by using surface-enhanced Raman spectroscopy. Analyst 142(10):1782–1789

12. Park J, Hwang M, Choi B et al (2017) Exosome classification by pattern analysis of surface-enhanced Raman spectroscopy data for lung cancer diagnosis. Anal Chem 89(12):6695–6701
13. Li X, Yang T, Lin J (2012) Spectral analysis of human saliva for detection of lung cancer using surface-enhanced Raman spectroscopy. J Biomed Opt 17(3):0370031–0370035
14. Huang Z, McWilliams A, Lui H et al (2003) Near-infrared Raman spectroscopy for optical diagnosis of lung cancer. Int J Cancer 107(6):1047–1052
15. Oshima Y, Shinzawa H, Takenaka T et al (2010) Discrimination analysis of human lung cancer cells associated with histological type and malignancy using Raman spectroscopy. J Biomed Opt 15(1):017009
16. Zheng XS, Jahn IJ, Weber K et al (2018) Label-free SERS in biological and biomedical applications: recent progress, current challenges and opportunities. Spectrochim Acta A 197:56–77
17. Zhang F, Braun GB, Shi Y et al (2010) Fabrication of Ag@ SiO2@ Y2O3: Er nanostructures for bioimaging: tuning of the upconversion fluorescence with silver nanoparticles. J Am Chem Soc 132(9):2850–2851
18. Brozek-Pluska B, Kopec M, Surmacki J et al (2018) Histochemical analysis of human breast tissue samples by IR and Raman spectroscopies. Protocols discussion. Infrared Phys Technol 93:247–254
19. Zhao J, Lui H, McLean DI et al (2007) Automated autofluorescence background subtraction algorithm for biomedical Raman spectroscopy. Appl Spectrosc 61(11):1225–1232
20. Hanlon E, Manoharan R, Koo T et al (2000) Prospects for in vivo Raman spectroscopy. Phys Med Biol 45(2):R1
21. Shetty G, Kendall C, Shepherd N et al (2006) Raman spectroscopy: elucidation of biochemical changes in carcinogenesis of oesophagus. Brit J Cancer 94(10):1460–1464
22. Krafft C, Neudert L, Simat T et al (2005) Near infrared Raman spectra of human brain lipids. Spectrochim Acta A 61(7):1529–1535
23. Ruiz-Chica A, Medina M, Sanchez-Jimenez F et al (2004) Characterization by Raman spectroscopy of conformational changes on guanine–cytosine and adenine–thymine oligonucleotides induced by aminooxy analogues of spermidine. J Raman Spectrosc 35(2):93–100
24. Chan JW, Taylor DS, Zwerdling T et al (2006) Micro-Raman spectroscopy detects individual neoplastic and normal hematopoietic cells. Biophys J 90(2):648–656
25. Stone N, Kendall C, Smith J et al (2004) Raman spectroscopy for identification of epithelial cancers. Faraday Discuss 126:141–157
26. Kaminaka S, Yamazaki H, Ito T et al (2001) Near-infrared Raman spectroscopy of human lung tissues: possibility of molecular-level cancer diagnosis. J Raman Spectrosc 32(2):139–141
27. Wu H, Xue R, Lu C et al (2009) Metabolomic study for diagnostic model of oesophageal cancer using gas chromatography/mass spectrometry. J Chromatogr B 877(27):3111–3117
28. Banki F, Yacoub WN, Hagen JA et al (2008) Plasma DNA is more reliable than carcinoembryonic antigen for diagnosis of recurrent esophageal cancer. J Am Coll Surg 207(1):30–35
29. Bergholt MS, Zheng W, Ho KY et al (2013) Fiber-optic Raman spectroscopy probes gastric carcinogenesis in vivo at endoscopy. J Biophotonics 6(1):49–59
30. Chowdary M, Kumar KK, Thakur K et al (2007) Discrimination of normal and malignant mucosal tissues of the colon by Raman spectroscopy. Photomed Laser Surg 25(4):269–274